Flow of the normal fluid component of He II about bluff objects observed with He_2^* excimers

X. Wen,[1,2,3] J. Pierce,[2] N. Lavrik,[4] S.J. Randolph,[4] W. Guo,[5,6] and M.R. Fitzsimmons[1,2,3,*]

[1]Department of Physics and Astronomy, University of Tennessee, Knoxville, TN 37996, USA.

[2]Oak Ridge National Laboratory, Oak Ridge, TN 37830, USA

[3]Shull Wollan Center—a Joint Institute for Neutron Sciences, Oak Ridge, TN 37830, USA

[4]Center for Nanophase Materials Sciences, Oak Ridge National Lab, Oak Ridge, TN 37830, USA

[5]Mechanical Engineering Department, FAMU-FSU College of Engineering, Florida State University, Tallahassee, FL 32310, USA.

[6]National High Magnetic Field Laboratory, Tallahassee, FL 32310, USA.

*Corresponding author: M.R. Fitzsimmons mfitzsi1@utk.edu

Abstract – Flow of the normal fluid component of He II about a cylinder and flat plate in a channel with square cross-section was observed by tracking clouds of He^* excimers. Flow was produced using a lithographically patterned heater. The direction and speed of flow projected onto a plane parallel to the axis of the channel and perpendicular to the heater exhibited significant change with time even after the heater was turned off. Flow was recorded in movies. Excimers moved at least as fast as could be recorded by the camera. Velocity vector field maps of flow suggest formation of structures ~~eddies~~ downstream of the cylinder object that are consistent with parts of eddies. This work establishes a foundation to observe normal component flow of a quantum fluid over centimeters.

purposes. DOE will provide public access to these results of federally sponsored research in accordance with the DOE Public Access Plan (http://energy.gov/downloads/doe-public-access-plan).

Introduction

Previously, Zhang and Van Sciver[1] observed flow of He II about a cylindrical bluff object using particle image velocimetry (PIV)[2,3,4,5] to record motion of many 1.7 μm diameter polymer spheres. The spheres, bluff object and He II were contained inside a channel-shaped cuvette. To induce flow a heater at the bottom of the cuvette was energized, and the surface of the He II actively pumped (cooled) to 2 K. For low heater power, smooth eddy-less flow was observed about the object. For high power, pairs of eddies in the wake and, remarkably, in front of the object (the latter displaced to the sides of cuvette) were observed. Eddies in the object's wake are expected for strong flow of a classical fluid; however, eddies in front of the object are not consistent with classical flow. Speculation at the time was that turbulence in front of the object was a manifestation of the unique properties of thermal counterflow between normal and superfluid components of He II.

Sergeev and Barenghi[6] analyzed two-dimensional Euler fluid flow past a disk. Using classical fluid dynamics, they obtained stationary solutions which allowed them to qualitatively conclude that quantized eddies exist upstream and downstream of the disk similar to those observed by Ref. [1]. Notably, mutual friction between normal and superfluid vortices was not required to produce eddies for the duration of the experiments. However, mutual friction would be required for quantized vortices to induce eddies in the normal component.

Later, Chagoverts and Van Sciver[7] reproduced the essential results of the previous experimental study—namely observation of smooth eddy-less flow for lightly driven counterflow and eddies

in front and behind the cylinder for strongly driven counterflow. For this work, He II was seeded with 1-5 μm diameter solid H_2 spheres, and the motion of individual spheres tracked using particle tracking velocimetry (PTV).[8,9,10,11] PTV enabled Chagoverts and Van Sciver[7] to observe H_2 tracers dragged by the normal fluid component of He II, and tracers trapped by quantum vortices in the superfluid component. Tracers in the two components were observed to move in opposite directions demonstrating thermal counterflow.

A year later, Duda et al.,[12] reported experimental results of thermal counterflow of He II past opaque and transparent cylinders using solid H_2 tracers under conditions like those of Refs. [1,7]. Duda et al., observed eddies in front and in the wake of the cylinder when the data were analyzed using PIV. However, they found no evidence for eddies in front of the object when the motion of the H_2 tracers was tracked using PTV. They suggested PIV tended to report vortices when none were observed with PTV. We note the observations of vortices were consistent for applications of PIV and PTV reported in Refs. [1,7].

Numerical simulations of thermal counterflow in He II about a cylinder provided insight into the physics leading to the formation of turbulence in a quantum fluid. Soulaine et al.,[13] found that for a ratio of superfluid ρ to normal fluid ρ densities, a __ 1, friction between the normal fluid component and the boundaries of the cuvette and object could induce eddies in the wake of the object for flow corresponding to modest heater power of Refs. [1,7,12]. For higher power, if the product of a and the mutual friction between normal fluid and superfluid components, γ, was sufficiently large, then eddies will form in front of the object. These simulations qualitatively explained the observations of Refs. [1,7]. Namely, mutual friction between superfluid and normal fluid components of He II is critical to the manifestation of

turbulence in front of a cylindrical bluff object. Understanding flow in such a fluid is important to applications such as cryogenic cooling of complex objects, e.g., accelerators,[14] or components having porous materials[15] (to maximize surface area in contact with the cooling medium).

A complexity of the experimental work to date is that massive tracers interact with both normal fluid and superfluid components of He II. Therefore, it is difficult to uniquely identify the origin of the eddies upstream of the cylinder. Do the eddies exist in the normal fluid component, or are the tracers trapped in polarized quantized vortices of the superfluid component? For temperatures >1 K, He^* excimers are only entrained by the normal fluid component,[16,17,18,19,20,21,22] so He^* excimers tracers can clarify the origin of eddies upstream of a cylinder in He II.[23,24,25,26] Other advantages of He^* excimer tracers in comparison to massive particles are: (1) the fluid can be seeded with excimers with less concomitant heating, and (2) interactions between excimers are relatively weak. For example, massive tracers may acquire electrostatic charge through friction between the gas flow and the injection-nozzle wall. We note electrostatic interactions are widely studied and exploited in the materials science of self-assembled small inorganic and organic (including polymeric) structures.[27,28,29,30]

In our two previous publications we reported a technique to produce He^* excimer molecules with neutron beams to seed a 1 cm by 1 cm by 1 cm volume of He II at the bottom of a long cuvette with square cross-section[31] and to observe thermally induced flow of excimer tracers in a channel filled with He II.[32] Through visual inspection of the fluorescence from He^* excimers, the excimers, and thus flow of the normal fluid component of He II, was observed to move vertically up the cuvette's channel away from the energized heater at the bottom of the cuvette. In addition, a machine learning algorithm identified clusters of excimers. The centroids of the clusters were tracked in a manner akin to PTV. The results yielded a velocity vector flow field

(in two dimensions) across an Eulerian grid. Here, we extend our studies to flow of the normal component of He II about two kinds of bluff objects—a cylinder and a flat plate. Because cooling the liquid/vapor surface opposite to the heater is not practical for our experiment (it is too expensive to pump and discard ^{3}He), the conditions of Ref. [1,7,12] cannot be faithfully reproduced. Thus, the long-term goal to determine whether eddies upstream of a cylinder occur only in the normal fluid component remains an outstanding challenge. Nevertheless, this work documents (1) the responsiveness of excimers to track the normal component of flow around objects on short (ms) time scales, (2) the consistency between raw recordings of the motion of excimer fluorescence around objects and velocity vector field maps obtained using machine learning and correlation analysis from the recordings, and (3) changes to the instrumentation that would yield an environment more closely replicating those described by Ref. [1,7,12] while preserving ^{3}He. This paper lays the foundation for future examination of the origin of eddies upstream of a cylinder bluff object using machine learning and recordings of He^* excimer fluorescence.

Methods

A detailed description of the experimental setup is given in Refs. [31, 32]. Briefly, an Oxford OptistatCF2 cryostat (a static exchange gas continuous flow cryostat) with quartz windows transparent to infrared light contained a 3.5 cm long quartz cuvette with a 1 cm by 1 cm cross-section. The cuvette was connected to a 3.5L reservoir filled with a mixture of ^{3}He and ^{4}He in the ratio of 1 to 99 (pressure was 97 kPa at 300 K). The cuvette was immersed in the liquid He bath (nominal temperature of 1.6 K), and the contents of the cuvette were cooled through the five walls of the cuvette.

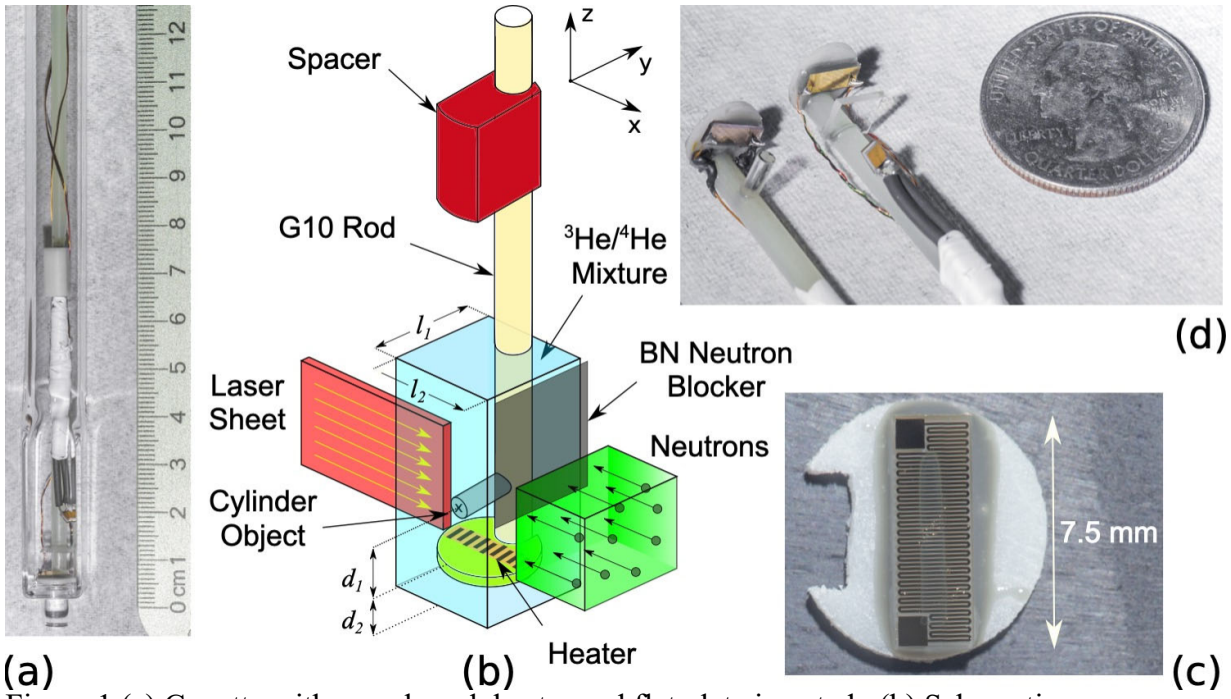

Figure 1 (a) Cuvette with sample rod, heater and flat plate inserted. (b) Schematic arrangement of the cuvette with respect to laser and neutron beams (l l 10 mm). The labyrinth heater (c) is d ~6 mm from the bottom of the cuvette (a). (d) Sample rods with glass cylinder and flat plate bluff objects installed d ~6 mm from the heater.

The instrumentation for the experiment (Figure 1) is most similar to that described in Ref. [32]; notably a BN beam blocker (outside the cryostat) blocked the neutron beam from entering the top half of the camera's field of view. A 343 Ω (at room temperature) labyrinth microheater was fabricated by photolithographically patterning gold onto a fused silica wafer. The wafer was subsequently diced into 2.5 mm by 7.5 mm chips (Figure 1(c)) that were secured to G10 pucks—only one was required for an experiment. The labyrinth was energized using a constant current source and provided a source of heat uniformly distributed across its 1.8 mm by 7 mm (plated) surface. The long dimension of the heater was parallel to the focal plane, laser plane and neutron beam incident vector (Figure 1 (b)). The heater was attached to a G10 rod and located 6 mm from the bottom of the cuvette. The G10 rod was displaced behind the focal plane by ~2 mm. A

bluff object (either a 2 mm diameter glass cylinder 4 mm long, or a 1 mm thick by 4 mm by 6 mm glass plate) was attached to the G10 rod ~6 mm above the heater (Figure 1(d)).

Because the liquid/vapor interface of the ^{3}He:^{4}He mixture was not actively pumped, the interface was not a cooling interface, thus, the flow of heat inside the cuvette may not be as simple as if the interface had been actively cooled. Nevertheless, as shown in Ref. [32], in the absence of a bluff object, the motion of the excimers is upwards implying the normal fluid component of He II flowed away from the heat source.

Results

We collected ~27 s of data taken at a rate of 55.6 Hz for heater powers of P 0, 2.5, 5, 7.5, 10, 15, 20, 30, 40, 60, 80 and 100 mW (heat flux q P/A, where A 0.13 cm^2 is the cross-section of the heater). Up to three 27-s-long measurements were taken for each power. All measurements used the same timing sequence: t 5 s neutron shutter open, t 8 s camera recording start, t 10 s lasers on, t 14 s heater on, t 18 s heater off, and t 35 s recording stop. During image acquisition, the temperature and ^{3}He:^{4}He vapor pressure sensors were recorded every 0.5 s. Prior to turning the heater on, the temperature of the cuvette equilibrated between 1.5 and 1.8 K. Just after the heater was turned off (t 18 s) the temperature of the cuvette increased by not more than 0.3 K compared to the temperature at t 14 s. In addition, a measurement with the neutron shutter closed (so no excimers were produced) and with the heater off was made using the same timing protocol. This measurement quantified the background, which was removed from the excimer fluorescence images in the manner described in the Supplemental Materials of Ref. [32].

He^* excimers were excited by 905 nm pulses with 4 ns duration at a rate of 1 kHz (9 mJ per pulse). Immediately after a pulse, each excimer will emit a 640 nm photon. We recorded the 640 nm fluorescence from He^* excimers during a 30 μs interval at a rate of 55.6 Hz with a camera that was synchronized with the laser. Because a photon has only a 1 in 42 chance of entering the solid angle subtended by the camera lens, we cannot continuously track individual excimers from frame to frame.[32] Because 10000's of excimers are created in a region reasonably confined by the path lengths of the proton and tritons (produced by ^{3}He absorption of a neutron), the excimers form clouds. Instead of tracking individual excimers, we track the fluorescence from clouds, or clusters of excimers. Clusters of excimers were identified using an unsupervised machine learning algorithm and the centroids of the clusters were tracked from frame to frame using a correlation metric.[32] A velocity vector flow field was constructed from the cluster/correlation analysis.

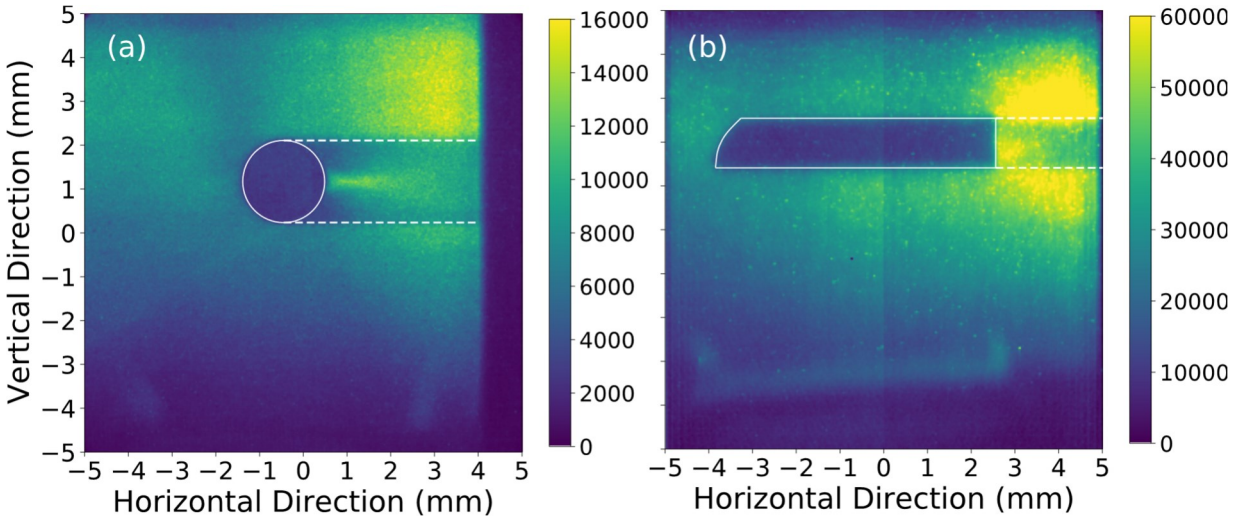

Figure 2 Exposure taken of He^* excimer fluorescence around the (a) cylinder (duration = 19 s) and (b) flat plate (duration = 25 s) bluff objects (outlined by continuous white lines). The 905 nm light used to excite the He^* excimers was refracted by the objects accounting for the nonuniformity of the fluorescence to the right of the objects and between the dashed lines. The BN neutron beam blocker was removed to acquire these images. The color bar shows the number of counts recorded in a pixel during the exposure. Counts are proportional to the charge accumulated by the pixel. Charge is proportional to the intensity of the fluorescence.

Non-uniformity of illumination—origin and consequences

Excimer fluorescence in the 1 cm by 1 cm field of view mapped onto a 1024 by 1024 array of pixels (high resolution mode) was recorded for >19 s about the cylinder (Figure 2(a)) and flat plate (Figure 2(b)). These recordings were made without applying power to the heater. The boundaries of the objects are highlighted by continuous white lines in the figures. Inside the regions occupied by the objects, there are no excimers and hence appear dark. To the right of the objects and between the dashed lines in the figures are regions that are generally darker than elsewhere. The regions of diminished fluorescence result from the loss of 905 nm laser light (the laser light needed to excite the excimers) due to refraction of the beam by the bluff object. The nonuniformity occurs rapidly across the dashed lines. The sudden loss of excimer fluorescence may affect the clustering algorithm, e.g., the calculation of the cluster centroid may be shifted

outside the affected region where there is more light. We regard the velocity vector fields (shown later) just to the right of the objects to be less reliable than elsewhere.

The second nonuniformity of the light is the gradual increase of light from left to right. This nonuniformity is a consequence of the absorption of the neutron beam by ^{3}He (the absorption length is ~4 mm for the concentration of ^{3}He and the average of the neutron beam wavelength from 2.8 to 5.8 Å[33]). As the neutron beam travels through the cell, the beam is absorbed so there are fewer He^* excimers produced on the left than the right, consequently, there are fewer excimers to fluoresce. Because the loss of fluorescence is gradual, the loss will not lead to erroneous results in clustering or the process to identify cluster motion. However, because there is less light on the left than the right, there are fewer clusters to follow the flow on the left, so the uncertainty of the flow will be larger on the left than the right.

Flow of He II about a cylinder observed with He^* excimers

To record flow of He II about the cylinder, a power P was selected for the heater, and a recording was made using the time sequence described earlier. For recordings of flow, the BN neutron beam blocker was placed outside the cryostat to the right of the camera's field of view. The blocker was positioned so that only the region of the cuvette for vertical position < 1 mm was illuminated by the neutron beam. We call the region below +1 mm, the excimer creation zone. Because excimers are not created above this zone, fluorescence above the zone must come from excimers that have moved upwards from the excimer creation zone into the shadow of the neutron beam.

Figure 3 shows images recorded with only background light subtracted—the latter measured with neutron beam shutter closed and heater off. Otherwise, the images were minimally

processed. Figure 3(a) is a collection of measurements from three experiments taken from t 10 to 14 s when the heater was off. This figure shows fluorescence was strongest *below* the neutron beam shadow, i.e., in the excimer creation zone. In this zone the intensity on the right is higher (yellow color) than the left (light green color), which is consistent with increasing absorption of the neutron beam from right to left. The relative absence of fluorescence in the neutron shadow (*above* the object) indicates the lack of flow to carry He^* excimers from the bottom to the top of the cuvette when the heater is off; however, diffusion of He^* excimers from bottom to top still occurs, contributing to some light in the neutron beam shadow. The diffusion length for He^* excimers at 1.6 K during the 5 s period from neutron shutter open to lasers on is ~1 mm.[34] The white line in Figure 3(a) shows the integration of the intensity over vertical position > 2 mm (i.e., *above* the object) vs. horizontal position. The zero of intensity for the line corresponds to the bottom of the figure.

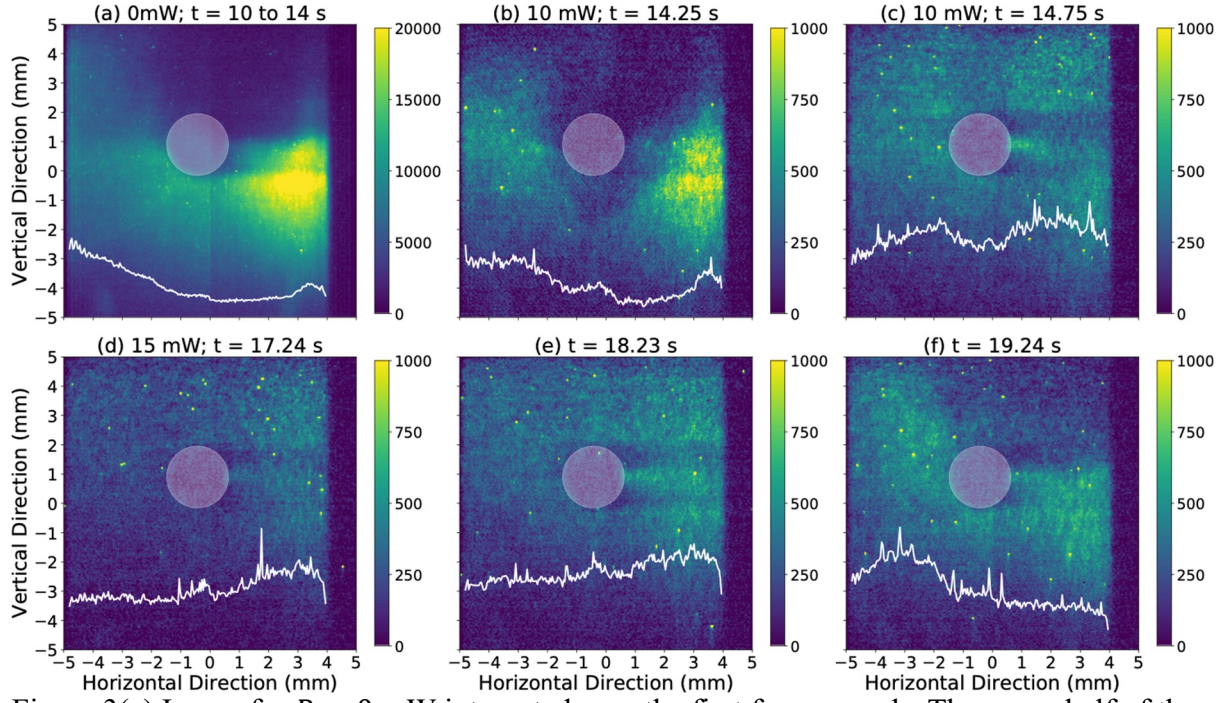

Figure 3(a) Image for P 0 mW integrated over the first four seconds. The upper half of the field of view is in the shadow of the neutron beam blocker (the beam blocker is to the right of the cryostat outside the field of view). Absence of light in this region implies the absence of flow. Images for P 10 mW integrated over a period of 0.5 s. These images show the wake of the cylinder devoid of light for (b) t 14.25 s, and then filling with light from excimers that flowed into the wake for (c) t 14.75 s. (b) and (c) were obtained from frames of the raw recording used to make Movie S1 of the Supplemental Materials.[35] A sequence of images for a measurement starting with P 15 mW (heater is on from t 14 to 18 s) integrated over a period of 0.5 s showing (d) low intensity of light in the upper half of the field of view, (e) more light with increasing intensity from left to right in the upper half, and (f) reversal of the distribution of light from left to right in the upper half compared to (d), thus evidence for circulation of excimer light and flow of the normal fluid component of He II around the cylinder. (d), (e), and (f) were obtained from frames of the raw recording used to make Movie S2 of the Supplemental Materials.[35] The white lines show the intensity integrated over vertical direction > 2 mm vs. horizontal direction. The scale of the white line ranges from zero to the same maximum for (b)-(f). The scale for (a) is 1/20th the scale for (b)-(f).

Figure 3(b,c) are 0.5 s integrations of data corresponding to P 10 mW for times of t 14.25 s and 14.5 s, respectively. Figure 3(b) shows the absence of fluorescence in the wake of the cylinder and then filling of the wake with fluorescence in Figure 3(c). This is evident by the broadly diminished intensity of the white line in Figure 3(b) corresponding to the integrated intensity in the plane above the object (vertical position > 2 mm). By "wake of the cylinder" we

mean the region above the cylinder and within ~ 3 mm of horizontal position = 0 mm. Then for Figure 3(c), the intensity in the region of vertical position > 2mm is more uniform vs. horizontal position—the broadly diminished intensity seen in Figure 3(b) being more tightly confined in Figure 3(c), and the variation vs. horizontal position being reduced.

Figure 3(d,e,f) show a sequence of 0.5 s time integrations of data starting with P 15 mW. Focusing on the upper half of the fields of view for the figures, and using the color bar as a guide to intensity of fluorescence, the intensity shown in the first image of the sequence (Figure 3(d)) is weak overall (in the range of ~250 to ~500 arbitrary units, a.u.). The left side is weaker than the right side as evident in the variation of the white line (intensity integrated over vertical position > 2 mm) of Figure 3(d). This observation is consistent with upwards flow of the normal fluid component of He II from the excimer creation zone in which there are fewer excimers on the left to trace the flow compared to the right. The intensity in the second image (Figure 3(e)) is somewhat stronger (in the range of ~375 to ~625 a.u.). The profile of the intensity above the object (the white line of Figure 3(e)) is higher than that of Figure 3(d), and the variation of the integrated intensity from left to right of the former is somewhat reduced compared to the latter. The intensity in the final image (Figure 3(f)) is highly non-uniform. The intensity ranges from a low of ~100 a.u. on the *right* side (upper corner) to a high of ~750 a.u. on the *left* side (upper corner). The variation from left to right is *opposite* to that of the first figure for the upper half of the field of view (compare the intensity profiles, i.e., white lines, of Figure 3(f) and Figure 3(d)). These images suggest that excimers moved (and thus the normal fluid component too) from right to left across the upper half of the field of view. These observations, as best a comparison of static images permit, are consistent with circulation of the normal fluid component flow in a counterclockwise direction about the cylinder.

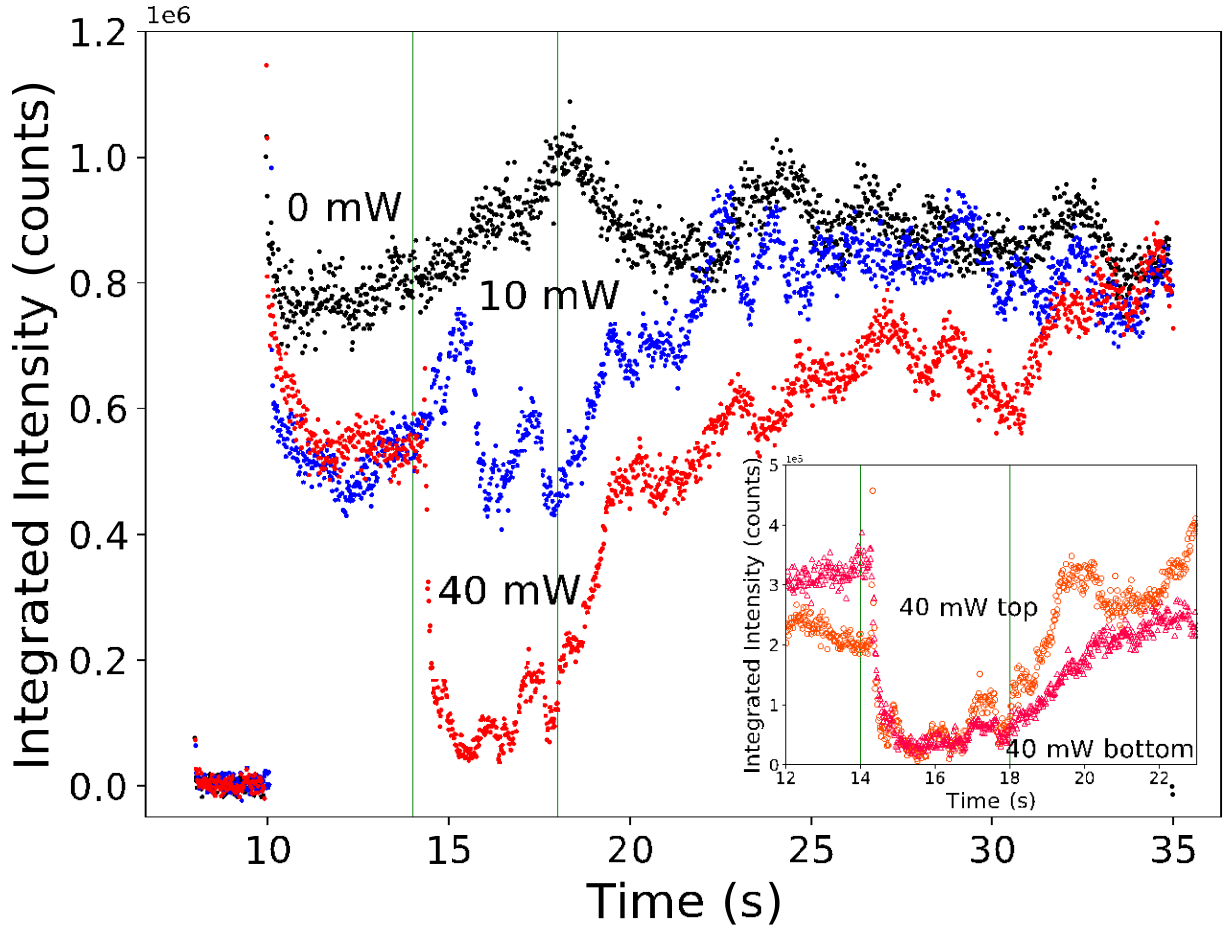

Figure 4 Intensity integrated over the entire field of view vs. time for P 0, 10 and 40 mW obtained from the cylinder object experiment. The faint green lines at t 14 and 18 s correspond to the times when the heaters were turned on and off, respectively (except for the P 0 mW measurement). (inset) Intensity integrated over the top (orange ○) and bottom (red Δ halves of the field of view vs. time for heater power of P 40 mW.

Movies for experiments corresponding to the static images are provided in the Supplemental Materials.[35] Data and movies for all powers are available on the Zenodo website.[36] Inspection of the movies (which is strongly encouraged) provides more clarity of the motion of the excimer light and hence the flow of the normal fluid component of He II. The feature that is most striking from the movies is how rapidly the light moves across the field of view. Notably, however, eddies are not evident from simple inspection of the movies. Defective camera pixels (amounting to 2.5% of the total number) were excluded from the movies. The movies show only

excimer peaks with intensities greater than three times the standard deviation of the background measurements (3σ). The excimer peaks in the movies will be used to identify clusters of excimers (discussed later).

Movies (see Supplemental Materials[35] and the Zenodo website[36]) show complex time-dependent flow of the fluorescence that persists after the heater is turned off. Figure 4 shows the intensity of the excimer light integrated over the entire field of view (after background subtraction) and over 0.5 s intervals vs. time. For the case of P 0 mW, the intensity varies by ~10%. For the cases of P 10 and 40 mW, the intensity varies more significantly. Note the strongly diminished intensity while the heater is on for the case of the P 40 mW data, and recovery of the intensity when the heater is turned off. This observation was consistently observed for all measurements taken with P 30 mW for the cylinder object.

Cluster analysis to deduce velocity vector flow fields around bluff objects

Velocity vector flow fields (projected onto the focal plane) can be deduced from superposition of many images of tracers that involve calculating cross-correlations between images (PIV) or tracking movement of individual tracers (PTV). Because the photon emitted by an excimer is unlikely to enter the camera, neither PIV nor PTV can be applied to directly track individual excimers for our experiment.[32] Instead, flow was inferred from motion of ensembles (clusters) of excimers, since these clusters contain many excimers and can produce enough photons to be recorded by the camera. A velocity vector flow field was deduced from the motion of the centroids accumulated during the time the heater was on (4 s), i.e., the flow field represents the net motion of flow during a 4 s interval.

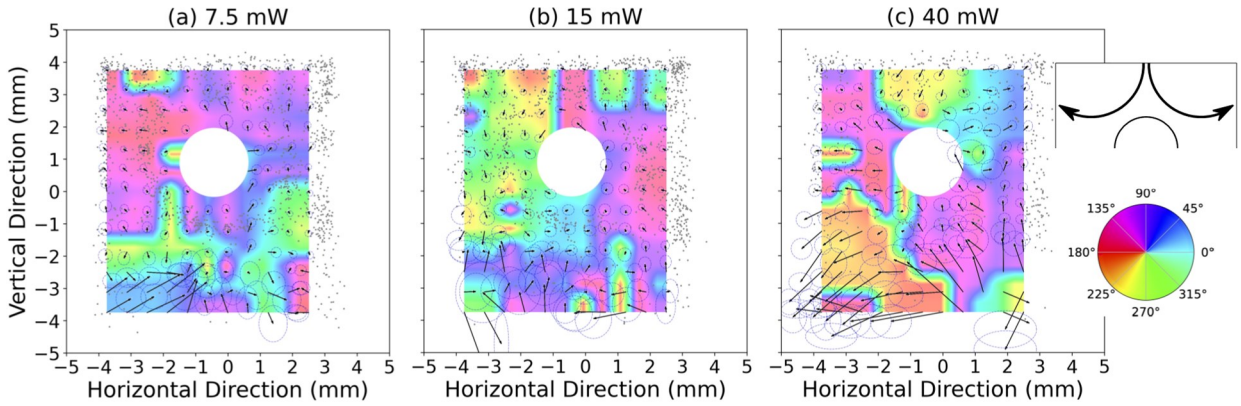

Figure 5 Correlated cluster pairs about the cylinder object are shown as gray dots for (a) *P* 7.5 (b) 15 and (c) 40 mW. A velocity flow field is shown by the arrows averaged over velocity vectors of the cluster pairs within a 2 mm by 2 mm integration window centered at each point of the Eulerian grid. The ellipses represent the uncertainty equal to the standard error of the mean for the vertical and horizontal components of the cluster pair velocities. Color represents the *direction* of the flow relative to the positive horizontal direction per the color wheel, inset lower right, with up being 90°. The flow as shown by the arrows and associated color in (c) (*P* 40 mW) is ~~schematically~~ indicated in the ~~cartoon~~schematic, inset upper right.

As described in Ref. [32], we applied an unsupervised machine learning (ML) algorithm to identify clusters of excimer light from every frame. The ML algorithm also returns the centroid of each cluster. A second algorithm (also described in Ref. [32]) identified pairs of centroids that were correlated frame to frame from which a displacement vector for each cluster pair was determined. Using the displacement vector and the frame rate of the camera, 1000+ velocity vectors were obtained for measurements while the heater was on. To facilitate visualization of the vector velocity flow field, an Eulerian grid with a mesh of 1 mm by 1 mm was defined,[32] and the average of the velocity vectors in a 2 mm by 2 mm integration window was obtained for each grid point. Results for a selection of heater powers is shown in Figure 5. The gray dots in the figure show the origin of the velocity vectors for the 1000+ cluster pairs. The black arrows show the direction and magnitude of the velocity for a grid point representing an average of cluster pair velocity vectors in the 2 mm by 2 mm integration window. The color wheel shows the *direction* of the flow in the manner used to show the spatial dependence of the orientation of the

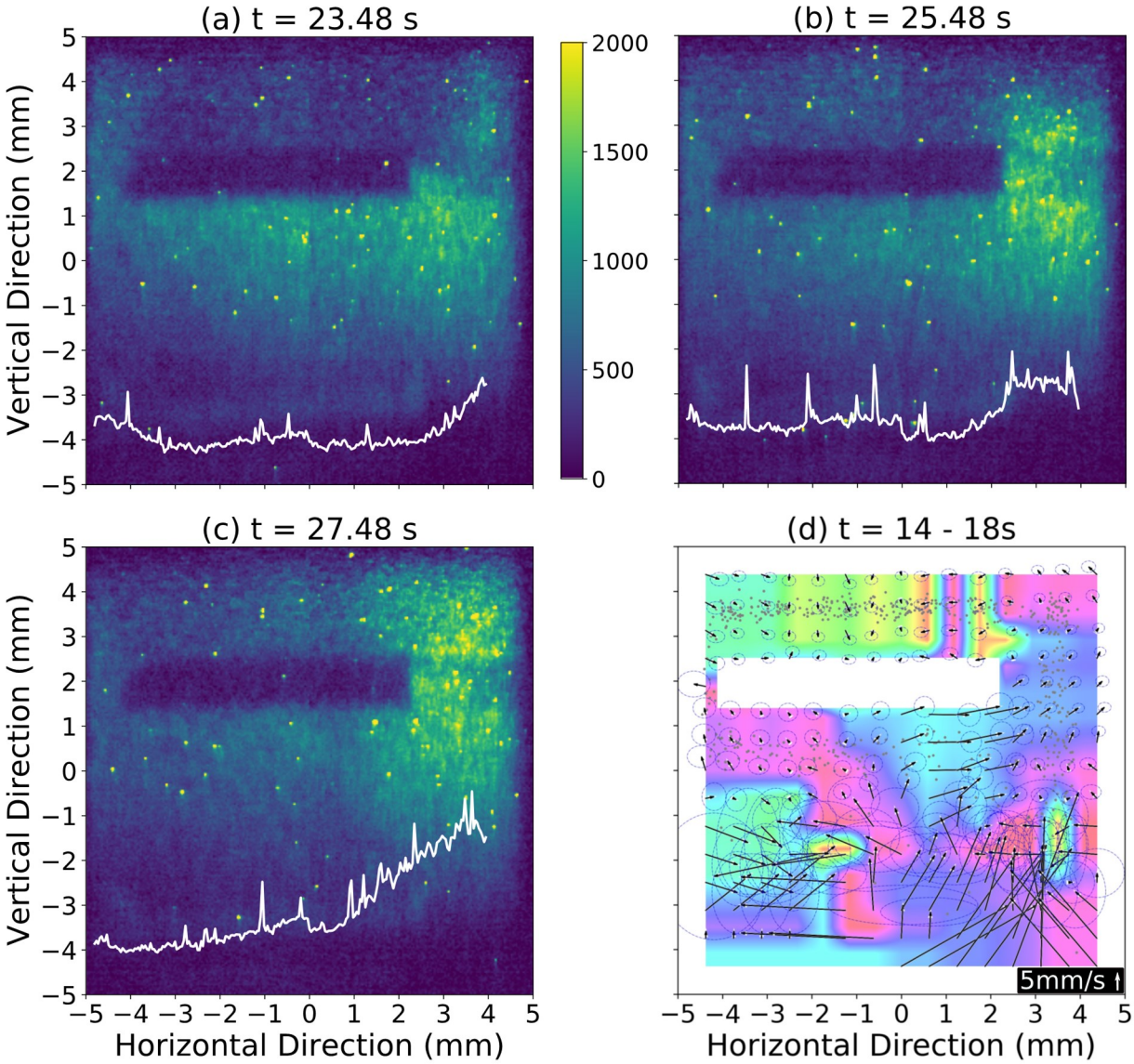

Figure 6 Excimer fluorescence taken in 2 s intervals showing movement of light from (a) left to (b) right under the flat plate and then upwards around the right edge of the plate from (b) to (c) occurring *after* the heater (*P* 20 mW) was turned off. (a), (b) and (c) were obtained from frames in Movie S3 of the Supplemental Materials.[35] (d) The velocity vector flow field obtained from measurements while the heater was on (*P* 20 mW) for a 4 s period. For meaning of color (direction of flow) refer to the color wheel shown in the inset of Figure 5.

vector magnetization of skyrmions.[37] Color is correlated with angle of the flow as measured relative to the horizontal direction pointing from left to right in the usual sense—angle is positive as measured in the counterclockwise direction. For example, a region of the figure colored "cyan" indicates the flow is moving parallel (0°) to the horizontal axis from left to right. The

velocity vector flow field provides a sense of magnitude and direction of flow compiled from 1000+ measurements over a 4 s period that otherwise might not be discernible by inspection of individual frames in movies by the eye.

Observations of normal fluid component flow were also obtained from images using a flat plate bluff object. Figure 6 shows a sequence of images integrated over 0.5 s taken at times of (a) t 23.48, (b) 25.48, and (c) 27.48 s. These times occur after the heater for P 20 mW *was turned off* (recall the heater was turned on at t 14 s for 4 s). These images show (a) fluorescence under the plate, (b) moving upwards next to the right edge of the plate, and then (c) along the top of the plate towards the left. The intensity profiles (white lines of intensity integrated over vertical position > 2.5mm vs. horizontal position), show the fluorescence to the right and above the plate increasing from (a) to (b) and then increasing above the plate towards the left of the right edge of the plate in (c). Note these images show motion that persisted after the heater was turned off. The motion of flow can also be observed in the velocity flow field in Figure 6(d) obtained from data taken while the *heater was on*. Counterclockwise flow around the right edge of the flat plate is evident by observing how the direction of the velocity vectors (Figure 6(d)) change as a path is traced starting at the bottom middle of the plate, then moving from left to right under the plate, then moving upwards along the right edge, then towards the left around the upper right corner of the plate. Similarly, the color in the region of the right edge of Figure 6(d), which depicts the direction of the velocity vectors, changes from cyan to blue to magenta to orange in this region transiting the color wheel (inset Figure 5) in the counterclockwise sense.

Discussion

The still images of Figure 3 and the field of view integrated intensity vs. time plot (Figure 4) exhibit remarkable changes in the position and intensity of the excimer fluorescence with time. Thus, the flow of the normal fluid component of He II must similarly change with time. Rough estimates for the components of the velocity of excimer motion can be extracted from the data in Figure 3. For P 10 mW (corresponding to q 770 W/m^2) and t 14.25 s, the wake above the cylinder is absent of excimer fluorescence (Figure 3(b)), and then at t 14.5 s the region is filled with light (Figure 3(c)). Assuming excimers flow into the ~6-mm-wide wake from either side, the horizontal component of the velocity is about ~6 mm/s $-6\ mm/0.5s$ for this time interval and power.

For P 40 mW, the intensity of the fluorescence (Figure 4(c)) changes dramatically. About 80% of the excimer light is lost 0.18 s after the heater was turned on at t 14 s. This implies many excimers left the 1 cm tall field of view at a rate of ~56 mm/s. Then, 1.5 s after the heater was turned off at t 18 s, the intensity recovered its initial value albeit at a slower rate. Because excimer light is a proxy for the flow of the normal fluid component of He II, the flow must rapidly change when the heater is turned on and off.

During the first 4 s of a measurement before the heater was turned on, there is no evidence for flow (Figure 3(a)); therefore, we assume for P 0 the velocity of flow is ~zero. Fitting values of v 6 1 ,56 6 mm/s corresponding to P 10 1 ,40 1 mW, respectively, to a line using orthogonal distance regression,[38,39] and the constraint: v 0 0 mm/s, yields an estimate of velocity in terms of power: v 1.0 1 P ——. This relation provides the reader with an estimate of velocity for a given power. For classical flow, the Reynolds number is given by Re ___, where ρ is the density of the medium, μ is the dynamic viscosity of the medium, and D is a

length scale characteristic of an object or channel.[40] Recognizing that He II is a quantum fluid, so application of a classical equation is perhaps dubious (see discussion of this point in Ref. [1]), we nevertheless provide an estimate of *Re*. Using ρ 0.145 g/cm^3 for the total density of the liquid, μ 1.3 10 Pa·s (for 1.6 K),[41] and setting D 2 mm (the diameter of the cylinder), we obtain Re 223 20 P/mW, which for our experiment means Re ranges from 0 to 22,300. This relation provides the reader with an estimate of the classical Re (of the normal fluid component) for a given power.

Even after the heater was turned off, the intensity of the fluorescence continued to oscillate by ~20% with a period of a couple of seconds (Figure 4). The diminished intensity for certain times after the heater was turned off means that He^* excimers moved outside the 1 cm by 1 cm field of view. After a couple of seconds, He^* excimers reappeared.

There are two sources of He^* excimers that can repopulate the field of view. One source is the creation of new He^* excimers in the bottom half of the cuvette (the excimer creation zone). This source can only partially replenish the He^* excimer population (corresponding to ^{3}He capture of a neutron at a rate of 1 s^{-1}). A second source is recirculation of the normal fluid component of He II from the top of the cuvette towards the bottom of the cuvette, thus bringing He^* excimers back into the field of view. To test this hypothesis, the I t data for P 40 mW are shown in the inset of Figure 4 integrated across the top (orange ○) and bottom (red Δ halves of the field of view separately. The intensity from the top half of the field of view recovers its t 10 s value 1.5 s after the heater was turned off (t 18 s). Whereas the intensity of the bottom half recovers its t 10 s value after 3 s. The factor of 2 longer time for He^* excimers to repopulate the bottom half of the field of view implies that He^* excimers primarily come into view from

above the field of view (as opposed to having been displaced in front/behind the laser sheet/focal plane or below the heater). Assuming He^* excimers move from the middle of the top half (of the field of view) to the middle of the bottom half (a distance of 5 mm) in 1.5 s, then we estimate the speed of the recirculation flow to be ~3 mm/s. We associate the rapid loss of excimer fluorescence (corresponding to a velocity of ~56 mm/s) for P 30 mW to the heat flux from the heater, and the return of the fluorescence when the heater is off to recirculation of flow from above the field of view.

Evolution of flow can add complexity to the interpretation of the velocity vector flow fields in Figure 5 and Figure 6(d). The flow fields were obtained from observations of cluster-centroid motion during 4 s periods when the heater was on for one to three experiments, thus, the flow fields represent the net flow while the heater was on. For the case of Figure 5(a), the net flow while the heater was on (P 7.5 mW) is upwards in the upper right corner corresponding to the blue-purple of the color wheel (90° as measured counter-clockwise relative to the positive horizontal direction of the field of view). On the upper left side, the flow is directed to the left side of the cuvette corresponding to red or 180°.

Figure 3(d,e,f) (P 15 mW) show a sequence of images in which the fluorescence rotates about the cylinder counterclockwise. If these images are representative of the entire 4 s period when the heater was on, then the flow field in Figure 5(b) (P 15 mW) should also exhibit a similar trend. Starting from the right side of the cylinder (Figure 5(b)) and moving counterclockwise around the cylinder, the color changes from purple to red to yellow to green to cyan—circumnavigating the color wheel in a counterclockwise direction. The flow field changes in the same manner as that observed in the still images and the movie of the fluorescence.[35,36]

Next, inspection of the rotation of the flow field for P 40 mW starting at *the middle of the top* of Figure 5(c), i.e., in the wake of the cylinder, shows a region on the left exhibiting clockwise rotation (yellow to red) and a region on the right exhibiting counterclockwise rotation (yellow to cyan). These counter-rotating circulations, structures, could be parts of ~~consistent with~~ a pair of counter-rotating eddies above (i.e., downstream) of the cylinder and centered above the camera's field of view. The combination of the vector field arrows and change of color above the object in Figure 5(c) is schematically shown in the upper right inset of the figure. ~~Only the bottom half of the eddies were observed (presumably their top halves would be above the field of view).~~ The directions of the ~~eddies~~ circulating flow is such that heat is transported to the cold vertical surfaces of the cuvette to the left and right of the cylinder. The heat flux from the heater for P 40 mW corresponds to 3 kW/m^2, and the average of the flow velocity magnitude above the cylinder is 2-5 mm/s. (The velocity of flow and the *Re* for classical flow at high power to produce eddies was noted to be less than that for eddy-free flow at lower power by Ref. [1].) The uncertainty of the flow (i.e., the sizes of the ellipses representing the standard error of the mean of the velocity vectors) is larger in comparison to the low power measurements, because there are fewer correlated-cluster-pairs when the heater was on for P 30 mW (80% of the excimer clusters were swept out of view). Nevertheless, eddies downstream of the cylinder object are anticipated for classical fluids for sufficiently large heat flux.[42]

In contrast to Refs. [1,7], we were unable to identify eddies upstream (in front of) the cylinder. There are several reasons why none were seen in our research that motivate future research. First, per the numerical simulations of Ref. [13], a value of a 1 is optimal to generate vortices in the wake of the object, and second, the mutual friction between superfluid and normal components should be large to generate vortices in front of the object. These conditions were

fulfilled by Refs. [1,7] which used temperatures of ~2 K just below the lambda point. Our experiment was performed significantly colder ~1.6 K for which $a \sim 5$. Thus, the conditions of our experiment were less conducive to formation of both types of vortices (although some of the data are consistent with vortices in the wake of the cylinder). In addition, the cuvette used by Refs. [1,7] was optimally suited to produce uniform heat flux by using a heater at the bottom of the cuvette and actively pumping on the liquid/vapor interface at the top. This situation is impossible to achieve using our technique which requires the He II to be spiked with ^{3}He, thus, pumping on the mixture is economically prohibitive. Heat flux in our system may not be as uniform as in Refs. [1,7].

The motion of the fluorescence implies complexity of the transport of He^* excimers by the normal fluid component. This is a situation that was not observed by Ref. [1] in recordings of polymer tracers in He II, nor in numerical simulations of Ref. [13] which suggested steady state should be achieved after ~4 s for the conditions of Ref. [1]. *N.b.,* we are not saying the previous results lack complexity, rather we are making a distinction between complexity of trajectories that are stable with time and those that are not.

In comparing our results with those of Ref. [1], we identified a here-to-fore unremarked feature in data from Ref. [1] arising from the stability of trajectories in time that is absent from our data. Code to produce our analysis of data in Ref. [1] is provided at our GitHub site.[43] Shown in Figure 7(a) is the integration of 100 images from the movie of the Supplemental Materials of Ref. [1]. A subset of the result is shown in Figure 7(b). Streaks of intensity, we call filaments, form either linear flow or circulating eddies. The filaments are separated by thin dark (i.e., low intensity) strips. The separation of the filaments in the region corresponding to vertical positions 14 to 20 mm is ~0.26(2) mm, i.e., nearest neighbor high intensity filaments are separated by

~0.26 mm wide regions of low intensity light. We monitored tracers transiting five pairs of light and dark regions of interest (ROI) measuring 44 μm by 44 μm as labeled in the image. In Figure 7(c) we plot the intensity vs. time recorded in the light (●) and dark (▽) ROIs (the intensity

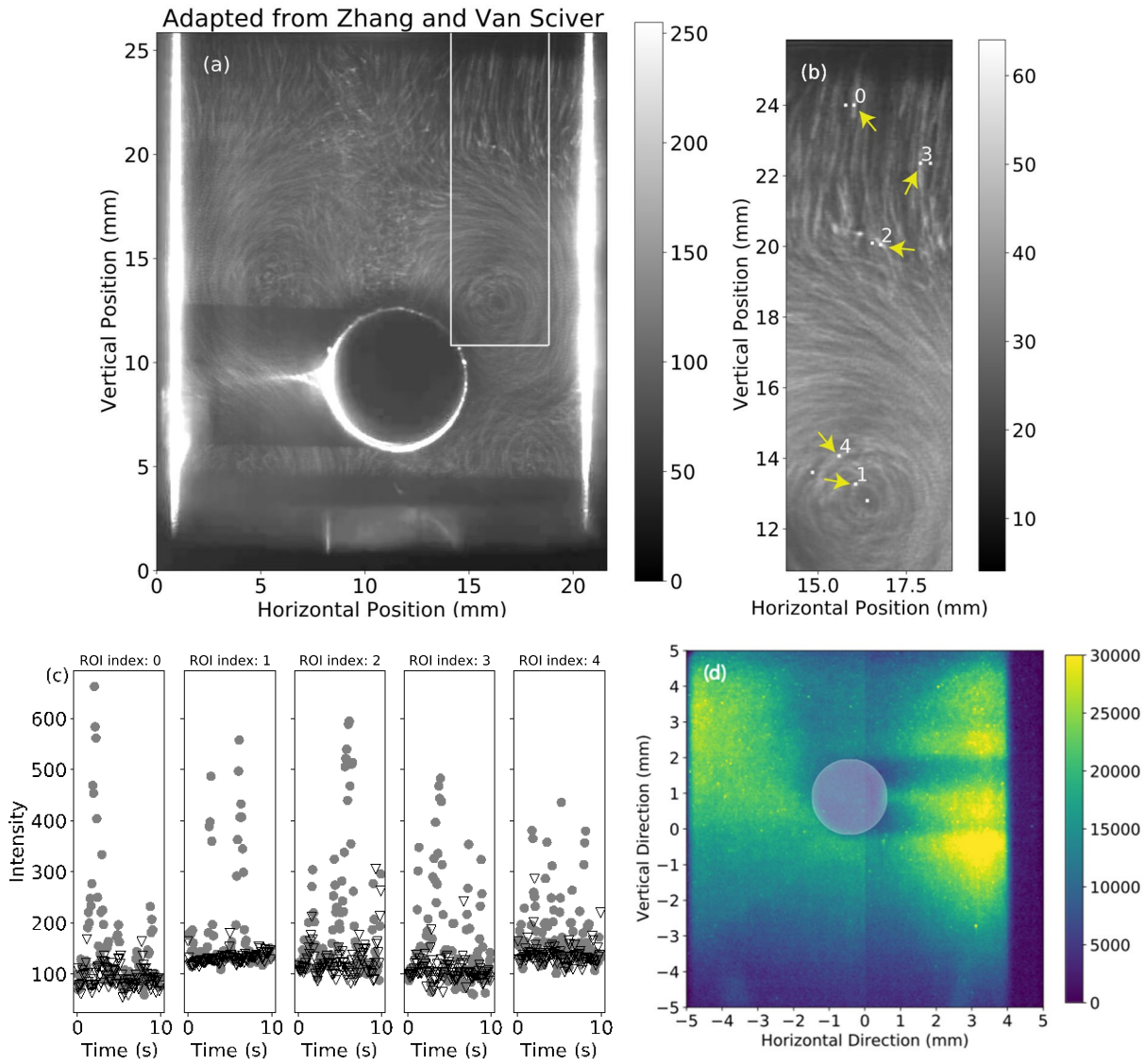

Figure 7 (a) Integration of 100 images from the movie of Ref. [1] for (q 11 kW/m^2, Re 21000). Region of the white box in (b) shows filaments of high intensity corresponding to light scattered by polymer spheres. The regions are labeled with numbers and pairs of white dots showing the locations of the bright and dark regions of interest. The locations of the bright ROIs are shown with arrows. The variations of intensity vs. time corresponding to tracers transiting 44 μm by 44 μm ROIs for light (●) and dark (▽) regions labeled in (b) are shown in (c). (d) Integration of 1000 images recorded for our experiment with conditions of P 100 mW (q 7.7 kW/m^2, $Re \sim 27000$) applied for 4 s during the 27 s measurement. Filaments were not observed in the He^* excimer fluorescence.

becomes high as a tracer transits the ROI). We found on average ~4 tracers travel through the light ROIs during the 10 s movie of Ref. [1] (~ 1 tracer per 2.5 s) and ~1 tracer though the dark ROIs during the same period. From inspection of the movie of Ref. [1], tracer motion in regions

corresponding to the light ROIs in Figure 7(b) exhibit speeds ranging from 4 to 10 mm/s. Using the time of ~2.5 s between tracers transiting the light ROIs and the velocity estimate, the spacings of tracers along a filament range from 10 to 25 mm—a large distance compared to the 20 mm width of the channel of Ref. [1]. An explanation could be a single tracer circumnavigates a closed filament (i.e., a loop), or different tracers enter the filament from different directions, e.g., perhaps from outside the focal plane of the camera. In any case, the physical spacing corresponding to tracer(s) transiting ROIs at different times is much larger than the physical separation between filaments, i.e., tens of mm compared to a quarter mm, respectively.

In contrast to the images shown in Figure 7(a,b), the integration of 200+ frames of a recording from our work (P 100 mW) with comparable heat flux q 7.7 kW/m^2 and $Re\sim22{,}300$ during a 4 s period from t 14 to 18 s (Figure 7(d)) shows no evidence for filaments, i.e., we see no tendency for He^* excimers to trace special paths. We put forward four hypotheses for the nonuniformity of the trajectories traced by the polymer spheres. (1) The polymers spheres may not have been seeded uniformly into the He II. (2) Repulsive interactions between the spheres, possibly of electrostatic origin, cause the spheres to be distanced from one another. (3) The spheres tend to follow each other for reasons analogous to why cyclists form a peloton (path of least resistance). (4) The trajectories are an example of a recurrent solution to the Navier-Stokes equation for fluid flow[44] realized by Ref. [1], but not by us.

Conclusions

In conclusion, we have observed flow of the normal component of He II around two bluff objects, a cylinder and a flat plate, by recording the motion of fluorescence of He^* excimers. For conditions of 1.6 K and heat flux of q 3 kW/m^2 (P 40 mW) producing thermal counterflow, we detected ~~eddies~~ counter-rotating circulations of flow with a tangential speed of

2-5 mm/s in the wake the cylinder object. These circulations could be parts of eddies downstream of the cylinder bluff. The classical Re for this condition is estimated to be ~8,900. We observed significant changes to the motion of excimer fluorescence and hence the normal component flow of He II with time, i.e., a steady state was not achieved during recordings lasting ~27 s. Even after the heater was turned off, the intensity of the fluorescence oscillated by about 20% every couple of seconds. For the cylinder study and high power, e.g., P 30 mW, nearly 80% of the He^* excimers were swept out of the field of view in ~0.2 s corresponding to a speed of tens of mm/s. The number of He^* excimers in the field of view recovered ~1 s after the heater was turned off. We attribute rapid changes of He^* excimer population (in the field of view) to the small inertia of the He^* excimers and their exclusive entrainment in the normal fluid component of He II, so they respond to rapid changes of flow of the normal fluid component about bluff objects in our cuvette. This work demonstrated the responsiveness of He^* excimers to track changing conditions of the flow of the normal fluid component of He II, and application of machine learning and correlation analysis to extract quantitative time-averaged two-dimensional velocity vector flow fields around objects.

Recently, we acquired images of a neutron beam using a next-generation event mode (Photonis brand[45]) camera with a Timepix3[46] chip. The camera had ps time resolution and consisted of 256 by 256 pixels with 55 μm by 55 μm pixel size and a maximum detection rate of 80 MHz integrated over the field of view.[47] The data collection requirements for the neutron beam demonstration far exceed those needed for the excimer experiment. With the new technology, we expect an increase of performance (and signal collection) by the ratio of the laser frequency to the frequency of the camera used presently of 1000 Hz/56 Hz = 18. A further 20x gain of signal can be achieved by using more ^{3}He and optimizing the field of view and camera lens.

Together the ~360x increased signal will improve the reliability of the clustering analysis strategy. An increased data acquisition rate (to 1 kHz) will also improve the reliability of the correlation analysis strategy and extend our ability to observe the responsiveness of excimers to changes of flow that occur in 1 ms instead of 18 ms.

Development and use of the lithographically patterned flat plate heater yielded more uniform heating compared to the coil heater used previously (see Ref. [32]). However, the lack of a cold surface opposite to the heater frustrates establishment of uniform heat flow for comparison with other work. One means to achieve such flow is to place the heater above the object and replace the glass bottom of the cuvette with a Cu plate. Owing to the low melting point of Cu compared to glass, the simple solution of making a glass to Cu seal at the bottom of the cuvette is not feasible. However, a glass to stainless steel flange could be fabricated, and an Indium seal used to connect a Cu plate to the stainless flange. This change would require a larger cryostat, yet the size of such a cryostat could still be smaller than the cross-section of the neutron beam (which can be ~100 cm^2 large).

Acknowledgments

This research used resources at the Spallation Neutron Source, a DOE Office of Science User Facility operated by the Oak Ridge National Laboratory. ORNL is managed by UT-Battelle, LLC, for the U.S. Department of Energy under Contract No. DE-AC05-00OR22725. Fabrication of the labyrinth heater was supported by the Center for Nanophase Materials Sciences (CNMS), which is a US Department of Energy, Office of Science User Facility at Oak Ridge National Laboratory. X.W. acknowledges support from the Shull Wollan Center Graduate Research Fellowship program and the Graduate Advancement, Training and Education program of University of Tennessee. W.G. acknowledges the support from the National Science Foundation

under Grant No. DMR-2100790 and the National High Magnetic Field Laboratory, which is supported by National Science Foundation Cooperative Agreement No. DMR-1644779 and the state of Florida.

---

[1] T. Zhang and S.W. Van Sciver, Nat. Phys. **1**, 36 (2005).

[2] R. J. Adrian and J. Westerweel, *Particle Image Velocimetry*, (Cambridge University Press, Cambridge, 2011).

[3] M. Raffel, C. Willert, S. Wereley, J. Kompenhans, *Particle Image Velocimetry: A Practical Guide.* (Springer-Verlag, Berlin, 2007).

[4] R. D. Keane and R. J. Adrian, Applied Scientific Research **49**, 191-215 (1992).

[5] R.J. Donnellly, A.N. Karpetis, J.J. Niemela, K.R. Sreenivasan, W.F. Vinen, and C.M. White, J. Low Temp. Phys., **126**, 327 (2002).

[6] Y.A. Sergeev and C.F. Barenghi, J. Low Temp. Phys., **156**, 268 (2009).

[7] T.V. Chagovets and S.W. Van Sciver, Phys Fluids **25**, 105104 (2013).

[8] Dana Dabiri and Charles Pecora, *Particle Tracking Velocimetry*, (IOP Publishing, Bristol, UK, 2019) https://doi.org/10.1088/978-0-7503-2203-4

[9] Kazuo Ohmi and Hang-Yu Li, *Meas. Sci. Technol.* **11**, 603 (2000).

[10] S. J. Baek and S. J. Lee, Experiments in Fluids **22**, 23 (1996)

[11] Y. Tang, S. Bao, T. Kanai, W. Guo, Phys. Rev. Fluids **5**, 084602 (2020).

[12] D. Duda, M. La Mantia, M. Rotter and L. Skrbek, J. Low Temp. Phys. **175**, 331 (2014).

[13] C. Soulaine, M. Quintard, B. Baudouy and R. Van Weelderen, Phys. Rev. Lett. **118**, 074506 (2017).

[14] Ph. Lebrun and L. Tavian, *Cooling with Superfluid Helium*, Proceedings of the CAS-CERN Accelerator School: Superconductivity for Accelerators, pp. 453-476 (2014).

https://doi.org/10.5170/CERN-2014-005.453

[15] S.W.K. Yuan, T.C. Nast, T.H.K. Frederking, Advances in cryogenic engineering. Vol. 35A - Proceedings of the 1989 Cryogenic Engineering Conference, Los Angeles, CA, July 24-28, 1989 (A92-13337 03-31). New York, Plenum Press, 1990, pp. 197-204.

[16] A. Marakov, J. Gao,W. Guo, S.W. Van Sciver, G. G. Ihas, D. N.McKinsey, andW. F. Vinen, Visualization of the normal-fluid turbulence in counterflowing superfluid ^{4}He, Phys. Rev. B **91**, 094503 (2015).

[17] J. Gao, W. Guo, V. S. L'vov, A. Pomyalov, L. Skrbek, E. Varga, and W. F. Vinen, Decay of counterflow turbulence in superfluid ^{4}He, JETP Lett. **103**, 648 (2016).

[18] J. Gao, W. Guo, and W. F. Vinen, Determination of the effective kinematic viscosity for the decay of quasiclassical turbulence in superfluid ^{4}He, Phys. Rev. B **94**, 094502 (2016).

[19] J. Gao, E. Varga, W. Guo, and W. F. Vinen, Energy spectrum of thermal counterflow turbulence in superfluid helium-4, Phys. Rev. B **96**, 094511 (2017).

[20] J. Gao, E. Varga,W. Guo, andW. F. Vinen, Statistical measurement of counterflow turbulence in superfluid helium-4 using He∗2 tracer-line tracking technique, J. Low Temp. Phys. **187**, 490 (2017).

[21] J. Gao, W. Guo, S. Yui, M. Tsubota, and W. F. Vinen, Dissipation in quantum turbulence in superfluid ^{4}He above 1 K, Phys. Rev. B **97**, 184518 (2018).

[22] S. Bao, W. Guo, V. S. L'vov, and A. Pomyalov, Statistics of turbulence and intermittency enhancement in superfluid ^{4}He counterflow, Phys. Rev. B **98**, 174509 (2018).

[23] D. E. Zmeev, F. Pakpour, P. M. Walmsley, A. I. Golov, W. Guo, D. N. McKinsey, G. G. Ihas, P. V. E. McClintock, S. N. Fisher, and W. F. Vinen, *Excimers He^* as Tracers of Quantum*

Turbulence in ^{4}He in the T = 0 Limit, Phys. Rev. Lett., **110** 175303 (2013). https://doi.org/10.1103/PhysRevLett.110.175303

[24] W. F. Vinen. *Quantum Turbulence: Where Do We Go From Here?,* AIP Conference Proceedings **850**, 169 (2006); https://doi.org/10.1063/1.2354655

[25] W. Guo. *Molecular Tagging Velocimetry in Superfluid Helium-4: Progress, Issues, and Future Development,* J. of Low Temp. Phys., **196**, 60 (2019). https://doi.org/10.1007/s10909-018-2102-1

[26] D. Mateo, J. Eloranta and G. A. Williams, *Interaction of ions, atoms, and small molecules with quantized vortex lines in superfluid ^{4}He*. J. Chem. Phys. **142**, 064510 (2015). https://doi.org/10.1063/1.4907597

[27] N.R. Visaveliya and J.M. Köhler, Adv. Func. Mater. **31**, 2007407 (2021).

[28] F. Nan, F. Han, N.F. Scherer, Z. Yan, Adv. Mater., **30**, 1803d238 (2018).

[29] S. Li, B.A. Moosa, J.G. Croissant, N.M. Khashab, Ang. Chemie, **54**, 6804 (2015).

[30] Z. Zhu, N. Xu, Q, Yu, L. Guo, H. Cao, X. Lu, Y. Cai, Macromolecular Rapid Comm., **36** 1521 (2015).

[31] X. Wen, Shiran Bao, L. McDonald, J. Pierce, G.L. Greene, Lowell Crow, Xin (Tony) Tong, A. Mezzacappa, R. Glasby, W. Guo and M.R. Fitzsimmons, Phys. Rev. Lett., **124**, 134502 (2020).

[32] X. Wen, L. McDonald, J. Pierce, W. Guo and M.R. Fitzsimmons, Scientific Reports, **12**, 20383 (2022).

[33] https://www.ncnr.nist.gov/resources/activation/

[34] W. Guo D.N. McKinsey, A. Marakov, K.J. Thompson, G.G. Ihas and W.F. Vinen, J. Low Temp. Phys., **171**, 497 (2013).

[35] Supplemental Materials this paper.

[36] https://doi.org/10.5281/zenodo.7199829

[37] X.Z. Yu, Y. Onose, N. Kanazawa, J.H. Park, J.H. Han, Y. Matsui, N. Nagaosa and Y. Tokura, Nature **465**, 901 (2010)

[38] http://www.mechanicalkern.com/static/odr_ams.pdf

[39] https://github.com/mfitzsimmons44/Fit-a-polynomial-to-data

[40] A. Sommerfeld, *A contribution to hydrodynamic explanation of turbulent fluid motions*, International Congress of Mathematicians, **3**, 116 (1908).

[41] Russell J. Donnelly, and Carlo F. Barenghi, *The Observed Properties of Liquid Helium at the Saturated Vapor Pressure,* Journal of Physical and Chemical Reference Data, **27**, 1217 (1998); https://doi.org/10.1063/1.556028

[42] D. J. Tritton, *Flow past a circular cylinder*. In: Physical Fluid Dynamics. (Springer, Dordrecht, 1977) pp. 18-29. https://doi.org/10.1007/978-94-009-9992-3_3

[43] https://github.com/xwen0518/Flow-of-the-normal-component-of-He-II-about-bluff-objects-observed-with-He-excimers

[44] C.J. Crowley, J.L. Pughe-Sanfor, W. Toler, M.C. Krygier, R.O. Grigoriev, M.F. Schatz, PNAS **119**, e2120665119 (2022). https://doi.org/10.1073/pnas.2120665119

[45] https://www.amscins.com/asi-photonis-joint-venture/

[46] https://kt.cern/technologies/timepix3

[47] https://zenodo.org/record/7231893